

# Brain State–Dependency of Coherent Oscillatory Activity in the Cerebral Cortex and Basal Ganglia of the Rat

Peter J. Magill,<sup>1</sup> Andrew Sharott,<sup>2</sup> J. Paul Bolam,<sup>1</sup> and Peter Brown<sup>2</sup>

<sup>1</sup>Medical Research Council Anatomical Neuropharmacology Unit, University of Oxford, Mansfield Road, Oxford OX1 3TH; and <sup>2</sup>Sobell Department of Motor Neuroscience and Movement Disorders, Institute of Neurology, Queen Square, London WC1N 3BG United Kingdom

Submitted 1 April 2004; accepted in final form 31 May 2004

**Magill, Peter J., Andrew Sharott, J. Paul Bolam, and Peter Brown.** Brain state–dependency of coherent oscillatory activity in the cerebral cortex and basal ganglia of the rat. *J Neurophysiol* 92: 2122–2136, 2004. First published June 2, 2004; 10.1152/jn.00333.2004. The nature of the coupling between neuronal assemblies in the cerebral cortex and basal ganglia (BG) is poorly understood. We tested the hypothesis that coherent population activity is dependent on brain state, frequency range, and/or BG nucleus using data from simultaneous recordings of electrocorticogram (ECoG) and BG local field potentials (LFPs) in anesthetized rats. The coherence between ECoG and LFPs simultaneously recorded from subthalamic nucleus (STN), globus pallidus (GP), and substantia nigra *pars reticulata* (SNr) was largely confined to slow- (~1 Hz) and spindle- (7–12 Hz) frequency oscillations during slow-wave activity (SWA). In contrast, during cortical activation, coherence was mostly restricted to high-frequency oscillations (15–60 Hz). The coherence between ECoG and LFPs also depended on BG recording site. Partial coherence analyses showed that, during SWA, STN and SNr shared the same temporal coupling with cortex, thereby forming a single functional axis. Cortex was also tightly, but independently, correlated with GP in a separate functional axis. During activation, STN, GP, and, to a lesser extent, SNr shared the same coherence with cortex as part of one functional axis. In addition, GP formed a second, independently coherent loop with cortex. These data suggest that coherent oscillatory activity is present at the level of LFPs recorded in cortico-basal ganglia circuits, and that synchronized population activity is dynamically organized according to brain state, frequency, and nucleus. These attributes further suggest that synchronized activity should be considered as one of a number of candidate mechanisms underlying the functional organization of these brain circuits.

## INTRODUCTION

The basal ganglia (BG) are a group of subcortical brain nuclei intimately involved in movement and cognition (DeLong 1990; Gerfen and Wilson 1996; Graybiel 1995). The cerebral cortex, the principal afferent of the BG, directly transfers information to the BG through the striatum and subthalamic nucleus (STN), but may also indirectly influence the BG by the globus pallidus [GP; or external segment of globus pallidus in primates (GPe)] and thalamus. Processed information is transmitted out of the BG through the substantia nigra *pars reticulata* (SNr) and entopeduncular nucleus [or internal segment of globus pallidus in primates (GPi)] to thalamus, and thence to cortex, and also to midbrain and brain stem nuclei (for review, see Smith et al. 1998).

Although much is known about the anatomy of cortico-basal ganglia circuits and the integration of cortical information at

the level of single striatal and STN neurons (Gerfen and Wilson 1996; Nambu et al. 2002; Smith et al. 1998), the way in which the activities of large populations of cortical and BG neurons are coordinated (i.e., the “functional organization” of these circuits) remains obscure. Single units alone are inadequate for investigating population activity because they represent only one level of functional organization of a given brain area and thus reflect only a limited part of the information processing (Bullock 1997; Pesaran et al. 2002). This may be of particular relevance in the BG, where the output nuclei and their efferent partners receive highly processed information converging from multiple cortical and subcortical loops (Alexander and Crutcher 1990; Smith et al. 1998). Recordings of local field potentials (LFPs), which better reflect coordinated population activity (Hubbard et al. 1969; Mitzdorf 1985), and single units from multiple sites have proved useful for investigating the functional organization of the neocortex, thalamus, and hippocampus (Buzsáki 2002; Contreras et al. 1997; Engel and Singer 2001; Engel et al. 2001). Data from humans implanted with deep brain electrodes for the treatment of Parkinson’s disease (PD) suggest that these techniques will also be informative in BG circuits (Brown 2003; Levy et al. 2002; Liu et al. 2002). Indeed, coherent or temporally coupled LFPs are often observed in sensorimotor cortex and BG during behavior (Brown 2003). Moreover, the coherence and frequency profiles of oscillatory LFPs recorded from the cortex and BG of PD patients vary with movement and levodopa treatment, suggesting that the population activity reflected in the LFP may be functionally significant (Brown et al. 2001; Cassidy et al. 2002; Kühn et al. 2004; Levy et al. 2002; Marsden et al. 2001; Williams et al. 2002).

The recording sites available in the human are necessarily limited to therapeutic targets, such as the STN, and recordings can be performed only in patients with abnormal movement control. The overall objective of the current work was to investigate functional connectivity using simultaneous recordings from the cortex and other strategic BG sites of healthy animals in different brain states. To this end, LFP and unit recordings were made in the urethane-anesthetized rat, a good model for determining the impact of extremes of cortical activity on the BG (Magill et al. 2000, 2001), enabling us to test the dependency of coherent activity on brain state. Changes in LFPs were investigated using frequency analysis techniques that favor the demonstration of oscillatory rather than stochastic synchronization (Halliday et al. 1995; Rosen-

Address for reprint requests and other correspondence: P. J. Magill, MRC Anatomical Neuropharmacology Unit, University of Oxford, Mansfield Road, Oxford OX1 3TH, United Kingdom (E-mail: peter.magill@pharm.ox.ac.uk).

The costs of publication of this article were defrayed in part by the payment of page charges. The article must therefore be hereby marked “advertisement” in accordance with 18 U.S.C. Section 1734 solely to indicate this fact.

berg et al. 1998), although the latter may also exist in cortico-basal ganglia circuits.

Three key hypotheses were tested. First, that there is extensive temporal coupling between the ECoG and basal ganglia LFPs. Second, such coupling varies with frequency and depends on brain state. Third, that the pattern of coupling is also dependent on the precise site of LFP recording in BG, compatible with a relative functional segregation between different elements of the cortico-basal ganglia circuitry.

## METHODS

### Electrophysiological recordings and labeling of recording sites

Experimental procedures were carried out on adult male Sprague-Dawley rats (Charles River, Margate, UK) and were conducted in accordance with the Animals (Scientific Procedures) Act, 1986 (UK) and the APS's *Guiding Principles in the Care and Use of Animals*.

Electrophysiological recordings were made in 12 rats (200–320 g). Anesthesia was induced with isoflurane (Isoflo, Schering-Plough, Welwyn Garden City, UK) and maintained with urethane ( $1.3 \text{ g kg}^{-1}$ , ip; ethyl carbamate; Sigma, Poole, UK), and supplemental doses of ketamine ( $30 \text{ mg kg}^{-1}$ , ip; Ketaset, Willows Francis, Crawley, UK) and xylazine ( $3 \text{ mg kg}^{-1}$ , ip; Rompun, Bayer, Germany), as described previously (Magill et al. 2000, 2001). All wound margins were infiltrated with the local anesthetic bupivacaine ( $0.75\%$  wt/vol; Astra, Kings Langley, UK) and corneal dehydration was prevented with application of Hypromellose eye drops (Norton Pharmaceuticals, Harlow, UK). Animals were then placed in a stereotaxic frame. Body temperature was maintained at  $37 \pm 0.5^\circ\text{C}$  with the use of a homeothermic heating device (Harvard Apparatus, Edenbridge, UK). Anesthesia levels were assessed by examination of the ECoG (see following text), and by testing reflexes to a cutaneous pinch or gentle corneal stimulation. Electrocardiographic (ECG) activity and respiration rate were also monitored constantly to ensure the animals' well being (see following text). Mineral oil or saline solution ( $0.9\%$  wt/vol NaCl) was applied to all areas of exposed cortex to prevent dehydration.

The ECoG was recorded via a 1 mm diameter steel screw juxtaposed to the dura mater above the right frontal cortex [AP:  $-4.5 \text{ mm}$ , ML:  $-2.0 \text{ mm}$  (Paxinos and Watson 1986)], which corresponds to the medial agranular field of the somatic sensorimotor cortex (Donoghue and Wise 1982) and referenced against an indifferent electrode placed adjacent to the temporal musculature (Fig. 1A). This and adjacent regions of cortex project to both striatum and STN, as demonstrated in anatomical and electrophysiological studies (Fujimoto and Kita 1993; Kolomiets et al. 2003; Magill et al. 2004; Smith et al. 1998), and thus, activity in these regions is of direct functional relevance. Raw ECoG was band-pass filtered ( $0.1\text{--}150 \text{ Hz}$ ,  $-3 \text{ dB}$  limits) and amplified ( $2000\times$ , NL104 preamplifier; Digitimer Ltd., Welwyn Garden City, UK) before acquisition. The ECG was differentially recorded by two silver wires inserted into the skin of the ipsilateral forelimb and hindlimb. Raw ECG was band-pass filtered ( $10\text{--}100 \text{ Hz}$ ) and amplified ( $5000\times$ , NL104; Digitimer) before acquisition. The chest movements accompanying respiration were recorded using a miniature accelerometer (AP19, Bay Systems, Somerset, UK) and charge amplifier (Type 5007; Kistler Instrumente AG, Winterthur, Switzerland). The signal from the accelerometer allowed the depth and rate of respiration to be accurately assessed on- and off-line.

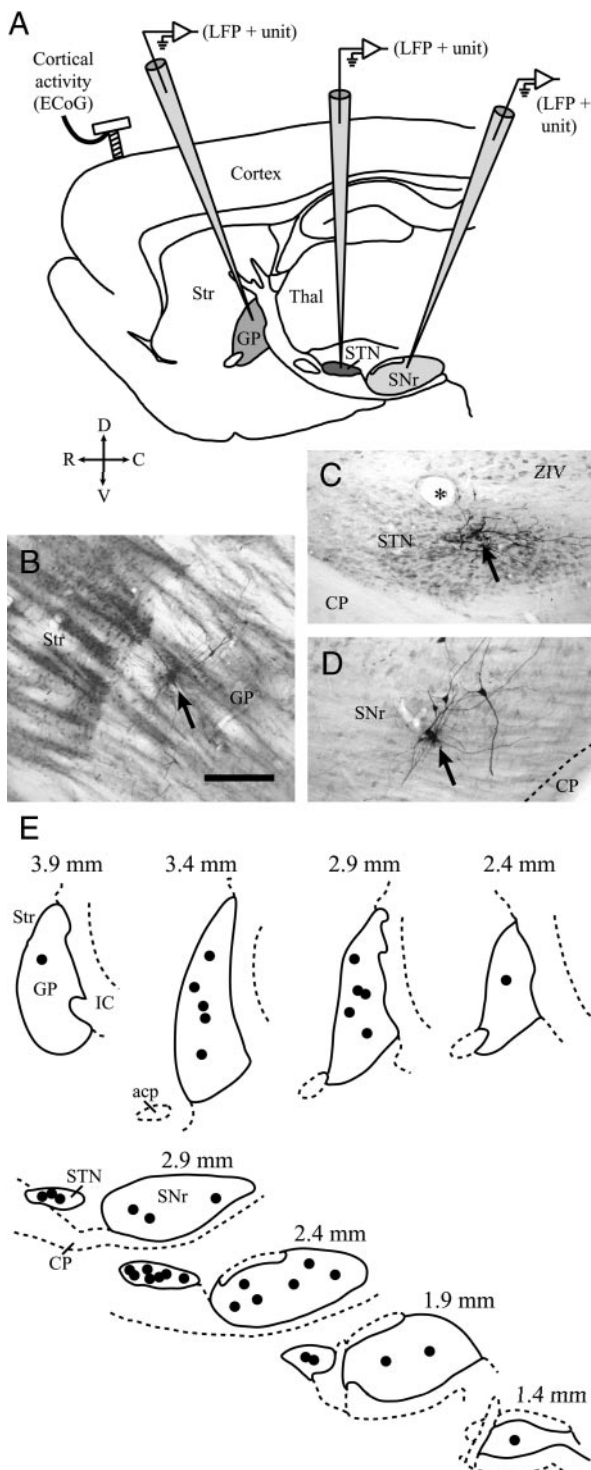


FIG. 1. Recording configuration and histological verification of recording sites. A: diagram of the recording configuration superimposed on a parasagittal section of rat brain. Local field potentials (LFP) and single-neuron (unit) activity were simultaneously recorded from the globus pallidus (GP), subthalamic nucleus (STN), and substantia nigra *pars reticulata* (SNr) of urethane-anesthetized rats, together with the ipsilateral frontal electrocorticogram (ECoG). Str, striatum; Thal, thalamus. B–D: digital images of histologically verified recording sites in GP, STN, and SNr from the same animal. B: GP recording site, indicated by an intense spot of black reaction product and Golgi-like labeling of neighboring neurons (arrow), was confirmed to be in the rostral portion of the nucleus, near the striatum. C: STN recording site was in the center of the nucleus (arrow), which lies dorsal to the cerebral peduncle (CP) and is characterized by a higher density of neurons compared with the overlying ventral division of the zona incerta (ZIV). A large blood vessel (\*) lies on the border between dorsal STN and ZIV. D: SNr recording site was centrally placed in the lateral portion of the nucleus (arrow), which lies dorsal to the CP (border indicated by dashed line). E: recording sites in GP, STN, and SNr in all 12 animals. Numbers above sections correspond to the distances lateral of midline. IC, internal capsule; acp, anterior commissure. Scale bar in B also applies to C and D =  $200 \mu\text{m}$ .

Extracellular recordings of LFPs and action potentials in the ipsilateral GP, STN and SNr were simultaneously made with glass electrodes (6–12 M $\Omega$  measured at 10 Hz in situ, tip diameters of 2.5–3.0  $\mu$ m; see Fig. 1A) that were filled with a 0.5 M NaCl solution containing 1.5% wt/vol Neurobiotin (Vector Labs, Peterborough, UK). Extracellular signals from the 3 electrodes were amplified (10 $\times$ ) through the active bridge circuits of 2 Axoprobe-1A amplifiers (Axon Instruments, Foster City, CA), bifurcated, and then differentially filtered to extract LFPs and unit activity. The LFPs were recorded after further amplification (100 $\times$ ; NL106 AC-DC Amp, Digitimer) and low-pass filtering (between d.c. and 150 Hz; NL125 filters, Digitimer). Single units were recorded after AC-coupling, further amplification (100 $\times$ ; NL106, Digitimer), and band-pass filtering (between 0.4 and 4 kHz; NL125, Digitimer). The monopolar glass electrodes were independently referenced by wires inserted into the skin at the top of the neck. Three HumBug units (Quest Scientific, Vancouver, Canada) were used in place of traditional “notch” filters to eliminate mains noise or “hum” at 50 Hz (Brown et al. 2002). Action potentials were typically between 0.3 and 0.8 mV in amplitude and always exhibited an initial positive deflection. Recordings of spontaneous activity typically lasted for 20–40 min.

Activity was recorded, first, during slow-wave activity (SWA), which accompanies deep anesthesia and is similar to activity observed during natural sleep, and second, during episodes of sensory-evoked “global activation,” which contain patterns of activity that are more analogous to those observed during the awake, behaving state [see review by Steriade (2000) and references therein]. Sensory stimulation and subsequent global activation were elicited by pinching the hindpaw for 15 s with serrated forceps that were driven by a standard pneumatic pressure, as described previously (Magill et al. 2000, 2001). The animals did not exhibit either a marked change in ECG/respiration rates or a hindpaw withdrawal reflex in response to the pinch.

After the recording sessions, all recording locations were marked by discrete, extracellular deposits of Neurobiotin [100 nA anodal current; 1 s (50%) duty cycle for 60 min; Magill et al. 2001, 2004]. After a period of 1–2 h for the uptake and transport of the Neurobiotin by neurons and glia at the recording sites, animals were given a lethal dose of ketamine anesthetic and perfused via the ascending aorta with 100 ml of 0.01 M phosphate-buffered saline at pH 7.4 (PBS), followed by 300 ml of 0.1% wt/vol glutaraldehyde and 4% wt/vol paraformaldehyde in 0.1 M phosphate buffer, pH 7.4, and then by 150 ml of the same solution without glutaraldehyde. Brains were then postfixed in the latter solution at 4 $^{\circ}$ C for  $\geq$ 12 h before sectioning.

### Histochemistry

Standard techniques were used to visualize the Neurobiotin deposits (see Magill et al. 2001). Briefly, the fixed brain was cut into 60  $\mu$ m thick sections in the parasagittal plane on a vibrating blade microtome (VT1000S, Leica Microsystems, Milton Keynes, UK). Sections were washed in PBS and incubated overnight in avidin–biotin peroxidase complex (ABC Elite; 1:100; Vector) in PBS containing 0.2% vol/vol Triton X-100 and 1% wt/vol bovine serum albumin (Sigma). After washing, the sections were incubated in hydrogen peroxide (0.002% wt/vol; Sigma) and 3,3'-diaminobenzidine tetrahydrochloride (0.025% wt/vol; Sigma) in the presence of nickel ammonium sulfate (0.5% wt/vol; Sigma) dissolved in Tris buffer (0.05 M, pH 8.0) for 15–30 min. Neurobiotin-filled neurons and glia were intensely labeled with an insoluble, black/blue precipitate (Fig. 1, B–D). Finally, sections were dehydrated, cleared, and mounted for light microscopy using standard techniques (Bolam 1992). The precise locations of all recording sites in the BG were histologically verified. The central and medial two thirds of the GP, and all regions of STN and SNr were sampled in this study (Fig. 1E).

### Data acquisition and analysis

Local field potentials and unit activity were sampled at 400 Hz and 10 kHz, respectively. The ECoG, ECG, and respiration signals were each

sampled at 400 Hz. All biopotentials were digitized on-line with a PC running Spike2 acquisition and analysis software (version 4; Cambridge Electronic Design, Cambridge, UK). Data from the recording session were first scrutinized for ECG and respiration artifacts. LFP data contaminated with ECG artifact were rejected. The occasional influence of a respiration artifact (1.5–2.5 Hz; see also Hu et al. 2002) in the LFPs was negated by partialization of coherence measures with the respiration waveform as the “predictor” (see following text). Artifact-free data were then visually inspected and epochs of robust cortical slow-wave activity (see Fig. 2) or global activation (see Fig. 3) were identified (Magill et al. 2000, 2001). Portions of the concurrently recorded spike trains composed of 250 spikes were isolated and used for statistical analysis of spontaneous unit discharge. The coefficient of variation (CV) of the interspike intervals, a value used widely as an indicator of regularity in point processes (Johnson 1996), was calculated (the lower the CV value, the more regular the unit activity). Mean firing frequency was calculated from the reciprocal of the mean interspike interval. Statistical comparisons of unpaired data were performed using the Mann–Whitney *U* test. Statistical comparisons of paired data (i.e., firing rates or CVs before and during global activation) were performed using the Wilcoxon signed-rank test. Multiple statistical comparisons of unit discharge in GP, STN, and SNr were performed using a one-way ANOVA, with a post hoc Bonferroni test or, when not appropriate (in cases of inhomogeneous variance; Levene test), using the Kruskal–Wallace *H* Test, together with a post hoc Dunn test for further definition (SPSS, Chicago, IL). The criterion for significance was the 95% level (unless stated otherwise). Data are expressed as means  $\pm$  SD. Auto- and cross-correlograms of action potentials (between 250 and 1,200 per neuron) were calculated and normalized according to standard methods and a bin size of 1, 5, or 10 ms (Abeles 1982; Perkel et al. 1967).

The ECoG and LFP<sub>1</sub>, denoted by subscripts *A* and *B*, respectively, were assumed to be realizations of stationary, zero-mean time series. Spike trains were assumed to be realizations of stationary, stochastic point processes and were denoted by subscript *C* (Perkel et al. 1967). All the processes were further assumed to satisfy a mixing condition, whereby sample values widely separated in time were independent (Brillinger 1981). The principal statistical tool used for the data analyses was the discrete Fourier transform and parameters derived from it, all of which were estimated by dividing the records into a number of disjointed sections of equal duration (exact number of data points sampled within each section, and the corresponding frequency resolutions are given in each figure legend). A Hanning window filter was used for all spectral analyses. Spectra were estimated by averaging across these discrete sections (Halliday et al. 1995). In the frequency domain, estimates of the power spectra of the ECoG,  $f_{AA}(\lambda)$ , LFP<sub>1</sub>,  $f_{BB}(\lambda)$ , and spike train,  $f_{CC}(\lambda)$ , were constructed, along with estimates of coherence,  $|R_{AB}(\lambda)|^2$  and  $|R_{BC}(\lambda)|^2$ , between ECoG and LFP<sub>1</sub>, and between LFP<sub>1</sub> and spike train, respectively. Coherence is a measure of the degree to which one can linearly predict change in one signal given a change in another signal (Brillinger 1981; Halliday et al. 1995; Rosenberg et al. 1989). It is without units and it is bounded from 0 to 1, with a coherence of 0 indicating nonlinearly related signals, and a value of 1 signifying two identical signals. Because coherence is a measure of the linear association between two signals, the ECoG/LFP waveforms must be phase-locked (temporally coupled) and their amplitudes must have a constant ratio to be coherent at any given frequency. The appropriate coherence estimates can be interpreted as providing an estimate of the contribution of ECoG to LFP<sub>1</sub> activity and vice versa. In the example of ECoG and LFP<sub>1</sub>, the coherence is calculated according to

$$|R_{AB}(\lambda)|^2 = \frac{|f_{AB}(\lambda)|^2}{f_{AA}(\lambda)f_{BB}(\lambda)}$$

where  $\lambda$  denotes the frequency and  $f_{AB}(\lambda)$  is the cross spectrum between *A* and *B*. In the time domain, the cumulant density function  $q_{AB}(u)$ , with LFP<sub>1</sub> as the reference signal, was estimated from the

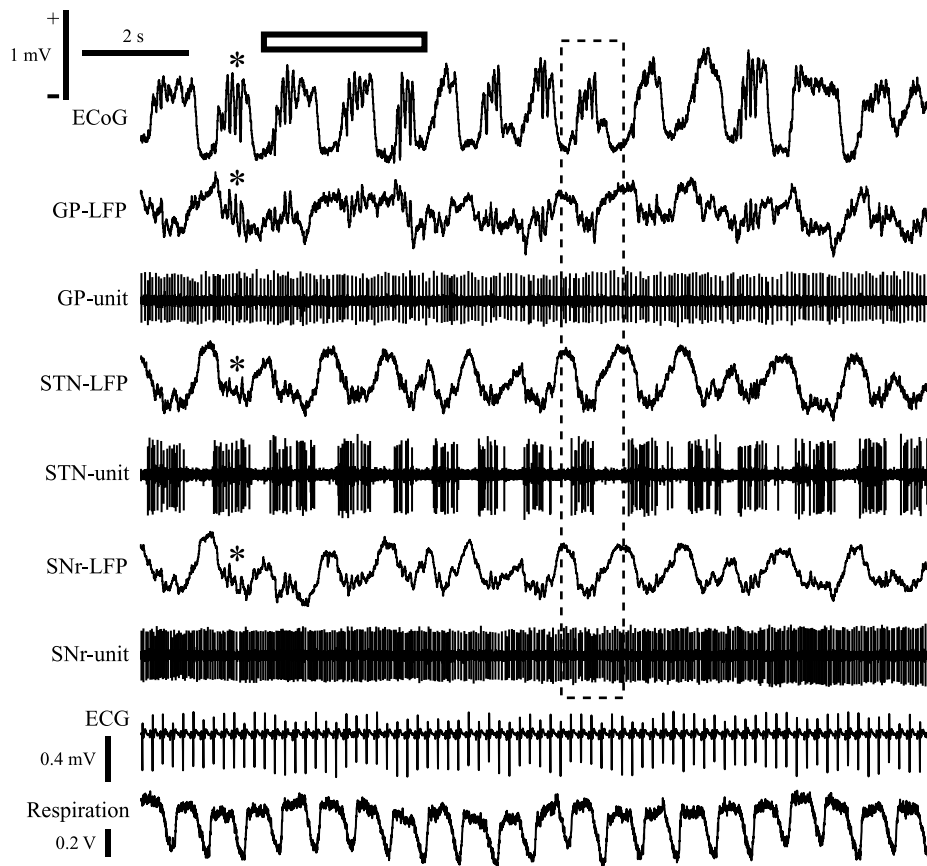


FIG. 2. Simultaneous recordings of activity patterns in the cerebral cortex and basal ganglia during robust slow-wave activity. ECoG was dominated by a large-amplitude, slow oscillation ( $\sim 1$  Hz) and spindle activity (7–12 Hz; one spindle is indicated by asterisks) during SWA. Concomitantly recorded LFPs in GP, STN, and SNr displayed similar oscillatory phenomena, but with reversed polarities compared with cortical activity (see dashed box for a clear example). Note that the LFP in GP did not reflect the cortical slow oscillation as faithfully as did LFPs in STN and SNr (see epoch under white bar for a clear example of this dissociation of signals). Neurons in STN exhibited low-frequency oscillations in firing and thus approximated a bursting type of activity. Such activity was closely related to the slow-wave activity in the ECoG and LFPs. Neurons in GP and SNr discharged at higher frequencies in a more regular manner, and the relationships between unit activity and ECoG/LFPs were not as clear as that in STN. ECoG and LFPs were not related to either electrocardiogram (ECG) or respiration. Calibration bars for ECoG apply to all basal ganglia recordings. Calibration bar for time also applies to ECG and respiration.

cross spectrum  $f_{AB}(\lambda)$  by an inverse Fourier transform. Similarly,  $q_{BC}(u)$ , with spike train as reference, was estimated from the cross spectrum  $f_{BC}(\lambda)$ . Cumulant densities provide a general measure of statistical dependency between random processes and will assume the value zero if the processes are independent (Halliday et al. 1995). They are similar to a cross-correlogram when comparing two zero-mean time series (e.g., relationship between ECoG and LFPs), or a

spike-triggered average when comparing a stochastic point process with a zero-mean time series (e.g., relationship between unit activity and corresponding LFP). Local field potentials were digitally low-pass filtered at 80 Hz for cumulant density estimates. For ease of interpretation, the y-axes of cumulant density estimates have been scaled in “correlation strength” (derived from the cross-correlograms between ECoG and LFPs) or  $\mu V$  (spike-triggered averages between units and

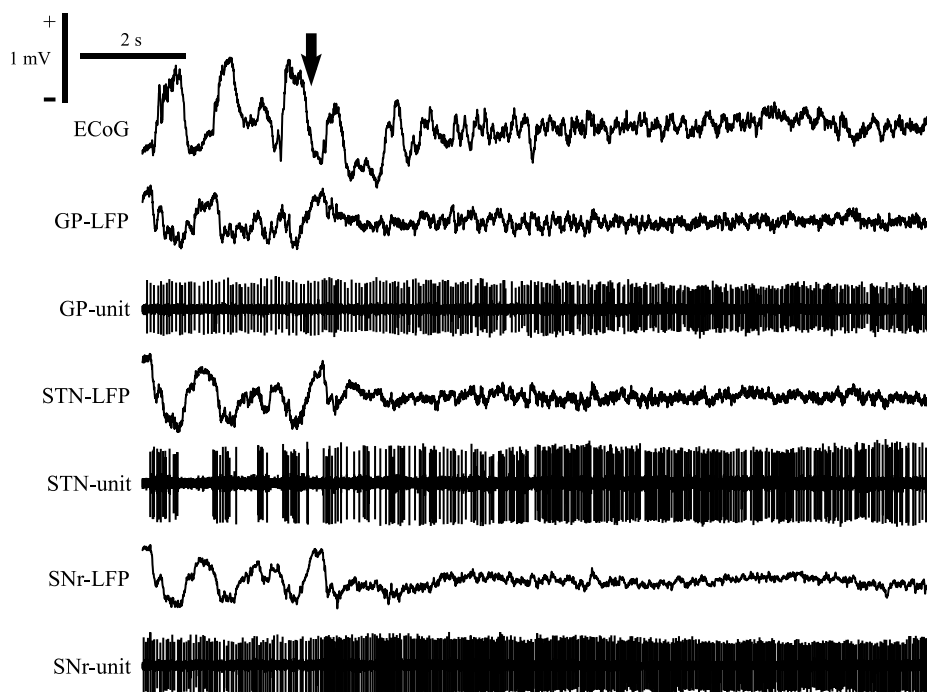
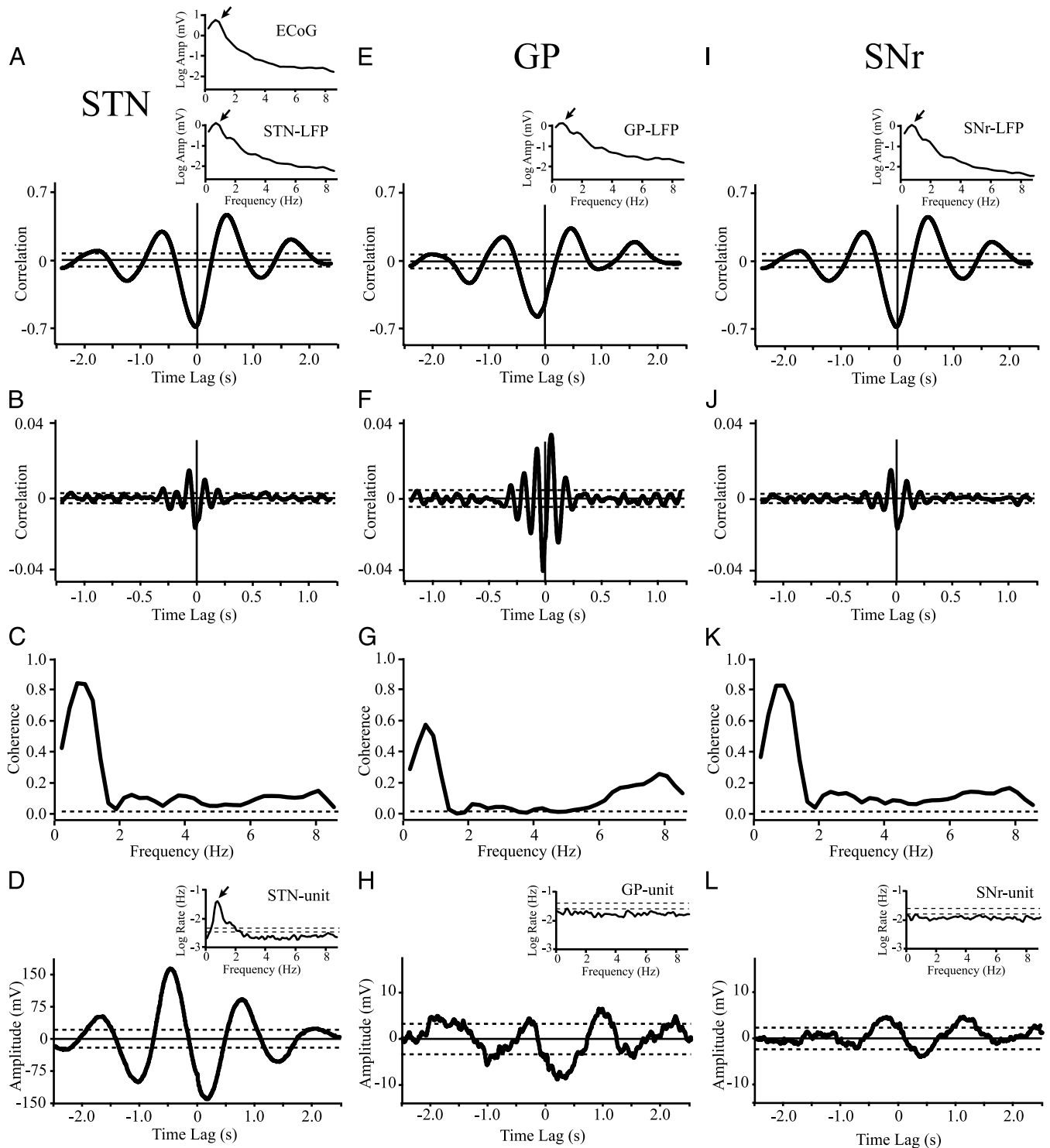


FIG. 3. Simultaneous recordings of activity patterns in the cerebral cortex and basal ganglia during global activation. Same recording sites and neurons as in Fig. 2. Global activation of the forebrain after pinch onset (arrow) was exemplified by a loss of slow-wave and spindle oscillations in the ECoG, and a shift to oscillatory activity of smaller amplitude and higher frequency. Local field potentials in GP, STN, and SNr displayed similar shifts in oscillatory phenomena. During global activation, the pattern of unit activity in STN switched from low-frequency oscillatory firing to tonic, regular/irregular firing at a higher frequency (CV of unit shown was reduced from 1.22 to 0.46; increase in firing to 180% of firing rate during SWA). Although the firing patterns of the GP unit and the SNr unit did not significantly change during activation, the firing rates of the neurons significantly increased (to 156 and 126% of firing rates during SWA, respectively). Calibration bars apply to all panels.

LFPs). Cumulant density estimates of SWA-related activity in basal ganglia were derived from long records (>5 min).

First-order partial coherence functions were estimated to assess whether "partialization" with a third process (hereafter referred to as the "predictor") accounted for the relationship between two other processes (Halliday et al. 1995; Rosenberg et al. 1989, 1998). The partial coherence can be viewed as representing the fraction of coherence between, for example, ECoG and STN-LFP that is not shared with a third signal, say GP-LFP. Thus if sharing of the signal between ECoG, STN-LFP, and GP-LFP were complete, then partial-

ization of the coherent activity between ECoG and STN-LFP with GP-LFP as the predictor would lead to zero coherence. It follows that if the coherent activity between ECoG and STN-LFP were kept completely separate from GP, partialization with GP-LFP as the predictor would have no effect on the coherence between ECoG and STN-LFP signals. For the present data, we examined the first-order partial coherence between the ECoG and LFP<sub>1</sub> after partialization with LFP<sub>2</sub> from another site as the predictor. The partialization of the coherence between ECoG and LFP<sub>1</sub> using the LFP<sub>2</sub>, denoted by subscript *D*, as predictor is denoted by  $|R_{AB/D} \lambda|^2$ . If LFP<sub>2</sub> contrib-



utes to coherence between ECoG and LFP<sub>1</sub>, then the partial coherence will show a clear reduction in magnitude compared with that of the ordinary coherence estimate between ECoG and LFP<sub>1</sub> over the relevant frequencies. Note that the partial coherence function is based on the assumption of linearity, so that failure in the partial coherence to decrease compared with the ordinary coherence does not exclude nonlinear interactions between the different signals. Example applications of first-order partial coherence functions to problems in neuroscience are given in Spauschus et al. (1999), Halliday et al. (1999), Kocsis et al. (1999), and Korzeniewska et al. (2003). Complete details of the analytic framework, including estimation techniques and procedures for the construction of confidence limits, are given in Rosenberg et al. (1989) and Halliday et al. (1995).

Coherence and partial-coherence analyses were performed on 2 data segments of activity during robust SWA episodes, as identified by assessing ECoG activity (see above), and one data segment of pinch-evoked activity per animal. All data segments were 80 s in length. Single data segments of pinch-evoked activity were derived by splicing together multiple recordings made during and immediately after (5 s) 4 hindpaw pinches. The variance of spectral power estimates was stabilized by logarithmic transformation (Halliday et al. 1995). To compare the coherence between signals, the variance of the modulus of the coherency (given by the square root of the coherence) was normalized using a Fisher transform (Rosenberg et al. 1989). Group analysis of transformed coherence data was performed by repeated-measures general linear models (GLMs) as described in the RESULTS. A Greenhouse–Geisser correction for nonsphericity was used where necessary and significance was set at  $P \leq 0.01$  to correct for the multiple GLMs. Post hoc testing was by 2-tailed paired *t*-test.

## RESULTS

### *Distinct patterns of cortical activity during SWA and global activation*

Cortical activity, as assessed from the ECoG, was the primary indicator of brain state. Two states were identified: slow-wave activity (SWA) and “global activation.” As described previously (Magill et al. 2000, 2001), urethane anesthesia was accompanied by regularly occurring slow waves of large amplitude ( $>450 \mu\text{V}$ ), with a mean frequency of  $0.89 \pm 0.12 \text{ Hz}$  ( $n = 12$ ), in the frontal ECoG (Fig. 2; see *inset* of Fig. 4A). Higher-frequency (7–12 Hz), smaller-amplitude ( $<200 \mu\text{V}$ ) spindle activity was often superimposed on the crests of the slow waves (Fig. 2).

Sensory stimulation by hindpaw pinch resulted in a marked loss of the power (i.e., rhythmicity and amplitude) of oscillatory activity in the slow- and spindle-frequency ranges in the ECoG (Fig. 3), indicative of global activation of the forebrain. This was paralleled by an increased presence of high-frequency, small-amplitude ( $<200 \mu\text{V}$ ) oscillations in the  $\beta$ - (15–30 Hz) and  $\gamma$ - (30–60 Hz) frequency ranges (Fig. 3).

### *Distinct patterns of basal ganglia LFPs during SWA and global activation*

Slow waves in the ECoG were associated with similar slow oscillations of large amplitude ( $>400 \mu\text{V}$ ) in the LFPs recorded from ipsilateral STN (mean peak frequency of  $0.90 \pm 0.12 \text{ Hz}$ ;  $n = 12$ ), GP ( $0.89 \pm 0.16 \text{ Hz}$ ), and SNr ( $0.90 \pm 0.13 \text{ Hz}$ ), as shown in Fig. 2 and *insets* of Fig. 4, A, E, and I.

Cumulant density estimates of ECoG and LFP activities confirmed that during SWA, the LFP and ECoG activities were correlated (Fig. 4, A, E, and I) and were dominated by a significant, rhythmic feature with a period of about 1 s (i.e.,  $\sim 1 \text{ Hz}$  oscillation). The surface-positive active components of the cortical slow oscillation were phase-locked, at small time lags, with deflections of negative polarity in all basal ganglia LFPs (Fig. 4, A, E, and I; also see epoch marked by dashed box in Fig. 2).

Spindle events in the ECoG were also reflected by similar oscillations in basal ganglia LFPs. As with classic cross-correlograms (Abeles 1982; Perkel et al. 1967), it may be difficult to resolve correlated activity of more than one frequency within cumulant density estimates. Indeed, large-amplitude common elements at low frequencies tend to dominate (Challis and Kitney 1990). To test for any correlation between ECoG and LFPs at spindle frequencies, the LFP signals were digitally high-pass filtered at 5 Hz. Under these circumstances, cumulant density estimates showed significant periodic features that repeated at intervals equivalent to a frequency of 7–12 Hz (Fig. 4, B, F, and J). These correlations were stronger for GP (Fig. 4F) than for STN (Fig. 4B) and SNr (Fig. 4J). Spindle oscillations in ECoG and basal ganglia LFPs were also of opposite polarities (Fig. 4, B, F, and J; also see epoch marked by asterisks in Fig. 2).

Global activation was always associated with time-locked changes in the profiles of LFPs recorded in basal ganglia (Fig.

FIG. 4. Oscillations in basal ganglia LFPs are temporally coupled to both ECoG activity and single-unit discharge during robust slow-wave activity. A, E, and I: cumulant density estimates (comparable to cross-correlograms) between the ECoG and the concomitant LFPs in STN (A), GP (E), and SNr (I). “Reference” signals were LFPs. Significant correlations at about 1 Hz were clearly evident. Note the small time lag between the ECoG and LFP in each case. *Insets*: power spectra of ECoG and LFPs both demonstrated significant peaks (arrows) at similar low frequencies (95% confidence limits were  $\leq 0.2 \log \text{ mV}^2$ ). B, F, and J: cumulant density estimates between the same LFPs (see A, E, and I), high-pass filtered at 5 Hz, and the concurrent ECoG. In each case, high-pass filtering the LFP removed the  $\sim 1 \text{ Hz}$  activity and revealed a significant periodic feature at spindle frequencies (7–12 Hz), which had a small time lag associated with it. Correlations at these frequencies tended to be greater in GP (F) as compared with STN (B) and SNr (J). C, G, and K: typical plots of the coherence between ECoG and the LFPs in STN (C), GP (G), and SNr (K). In each case, a large peak in coherence was seen at slow oscillation frequencies ( $\sim 1 \text{ Hz}$ ), although the coherence between ECoG and GP-LFP was consistently less than the coherence between ECoG and STN-LFP or ECoG and SNr-LFP. Smaller peaks were present at spindle frequencies. D, H, and L: cumulant density estimates (comparable to spike-triggered averages) between single units in STN (D), GP (H), and SNr (L), and the concurrent LFP (as shown in the *insets* in A, E, and I). “Reference” signals were unit activity. Significant temporal coupling between STN-unit and STN-LFP was present during slow-wave activity, with the unit tending to fire near the negative trough of the LFP oscillation (D). Temporal couplings between GP-unit and GP-LFP (H), and between SNr-unit and SNr-LFP (L), were weaker during slow-wave activity compared with coupling between STN-unit and STN-LFP, but were still significant. *Insets*: power spectra of the unit discharges showed a significant low-frequency oscillatory component (arrow) of unit activity in STN, but not GP or SNr. Data in A–L were taken from the same epoch of slow-wave activity (306 s of data, block size of 4096 data points, frequency resolution of 0.24 Hz); ECoG, LFPs, and units were simultaneously recorded. Dashed lines in the coherence spectra, cumulant density estimates, and single-unit power spectra are the 95% confidence limits.

3). Indeed, the loss of cortical SWA and the adoption of high-frequency, small-amplitude oscillatory activity in ECoG during sensory stimulation were effectively mirrored by similar shifts in the activity patterns of STN-LFPs, GP-LFPs, and SNr-LFPs (Fig. 3). Low-frequency, large-amplitude oscillatory activity in basal ganglia LFPs resumed only when SWA reappeared in the ECoG (data not shown).

#### *Coherence between ECoG and basal ganglia LFPs differs across brain states and frequencies*

Spontaneous activity in cortex and basal ganglia was significantly coherent in the slow-oscillation and spindle-oscillation frequency ranges during SWA (Fig. 4, C, G, and K; also see Fig. 5, A–C). Coherence analysis also confirmed that spontaneous activity in cortex and basal ganglia was significantly coherent at high frequencies that broadly encompassed  $\beta$ - and  $\gamma$ -band oscillations (15–60 Hz) during the activated brain state (Fig. 6, A–C), mirroring the loss of SWA and the adoption of high-frequency, small-amplitude activity in ECoG.

A general linear model (GLM) incorporating basal ganglia nucleus, frequency band, and brain state as the main effectors of activity relationships was used to assess differences in coherence between cortex and basal ganglia. There was no significant effect for nucleus correlated to ECoG (3 levels: STN, GP, and SNr), but there were significant effects for brain state (2 levels: SWA and global activation) and frequency (2 levels: 0.8–1.5 and 15–60 Hz). In addition, there were significant interactions between nucleus and frequency, and between brain state and frequency. There was no second-order interaction between nucleus and state, and no third-order interaction between nucleus, frequency, and state. Post hoc paired *t*-test confirmed that coherence in the 0.8- to 1.5-Hz band was significantly greater during SWA than during global activation for STN, GP, and SNr (compare Figs. 5 and 6), which is in good agreement with differences in the distribution of power of oscillatory activity in the two states. The average strength of coherence between LFPs and ECoG over the 0.8–1.5 Hz frequency band was greater for both STN and SNr than for GP (Fig. 5, A–C, insets). Coherence in the 15–60 Hz band was significantly larger for all BG nuclei during activation than during SWA (compare Figs. 5 and 6). Furthermore, the magnitude of coherence with cortex over the 15–60 Hz range was significantly greater for both STN and GP than for SNr (Fig. 6, A–C).

During robust SWA, there was also significant coherence between oscillatory activity in cortex and basal ganglia at frequencies associated with spindling (7–12 Hz; Fig. 5, A–C). Most of the coherence at spindle frequencies was lost during global activation (Fig. 6, A–C). A separate GLM was used to investigate whether there were any differences in coherence between ECoG and basal ganglia LFPs at slow-wave and spindle frequencies. The main factors were nucleus (3 levels: STN, GP, and SNr) and frequency band (2 levels: 0.8–1.5 and 7–12 Hz). Frequency was the only significant main effect, but there was also an interaction between nucleus and frequency. Post hoc *t*-test showed that coherence with ECoG at spindle frequencies was greater in GP than in STN or SNr, which both had similar levels (Fig. 5, A–C), in congruence with the cumulant density estimates of LFP and ECoG activities (Fig. 4). In general agreement

with previous studies showing that  $\beta$ - and  $\gamma$ -rhythms are often present during the active components of the cortical slow oscillation (Steriade 2000), there was low, but statistically significant, coherence between cortex and basal ganglia in the 15- to 60-Hz range during SWA (Fig. 5, A–C). In summary, coherence between cortex and basal ganglia was relatively frequency-selective. Differences in spectral power mirrored differences in coherence (Fig. 4), demonstrating that changes in coherence were not attributed to modulations in nonlinearly related frequency components (Florian et al. 1998).

#### *Pattern of coherence between ECoG and basal ganglia LFPs varies with recording site during SWA*

Partial coherence analysis was used to further define the functional organization of coherent activity between cortex and basal ganglia nuclei. During robust SWA, partialization of ECoG-STN coherence with the SNr signal as predictor (Fig. 5G) and partialization of ECoG-SNr coherence with the STN signal as predictor (Fig. 5F) markedly attenuated coherence at slow-wave frequencies (0.8–1.5 Hz), the dominant band of coherence. In contrast, partialization of either ECoG-STN coherence or ECoG-SNr coherence with GP acting as the predictor led to little change in coherence in this frequency band (Fig. 5, D and I, respectively).

Partialization of ECoG-GP coherence with either STN (Fig. 5E) or SNr (Fig. 5H) had a paradoxical effect in that coherence at slow-wave frequencies shifted, with a significant peak appearing at 2–3 Hz that was not evident in the standard mean ECoG-GP coherence spectrum (Fig. 5B). This occurs because ECoG-STN coherence and ECoG-SNr coherence are stronger than ECoG-GP coherence at slow-wave frequencies (compare Fig. 5, A–C) and implies that there is little temporal coupling of this component between STN/SNr and GP. Under these conditions, removal of the STN/SNr effect by partialization is equivalent to eliminating a “noise term” from the ECoG-GP coherence (Lopes da Silva et al. 1980). Removing this noise term leads to a relative increase of the frequency components shared by ECoG and GP, which appear at a slightly higher frequency.

In summary, the partial spectra in Fig. 5, D–I suggest that, during robust SWA, the cortex, STN, and SNr are temporally coupled at low frequencies in functional loops, which together form an axis of coherence that is largely independent of GP, which has its own independent activity that is coherent with cortex. Interestingly, this distinction between the cortex–STN–SNr and cortex–GP axes was less acute at spindle frequencies (7–12 Hz), where, for example, partialization of ECoG-SNr coherence or ECoG-STN coherence with the GP signal reduced coherences in this band, despite having little effect on coherences over the 0.8–1.5 Hz range (see Fig. 5, D and I, respectively).

#### *Pattern of coherence between ECoG and basal ganglia LFPs varies with recording site during global activation*

During global activation, ECoG-STN coherence and ECoG-SNr coherence, which were mainly confined to the 15–60 Hz band, were significantly reduced after partial-

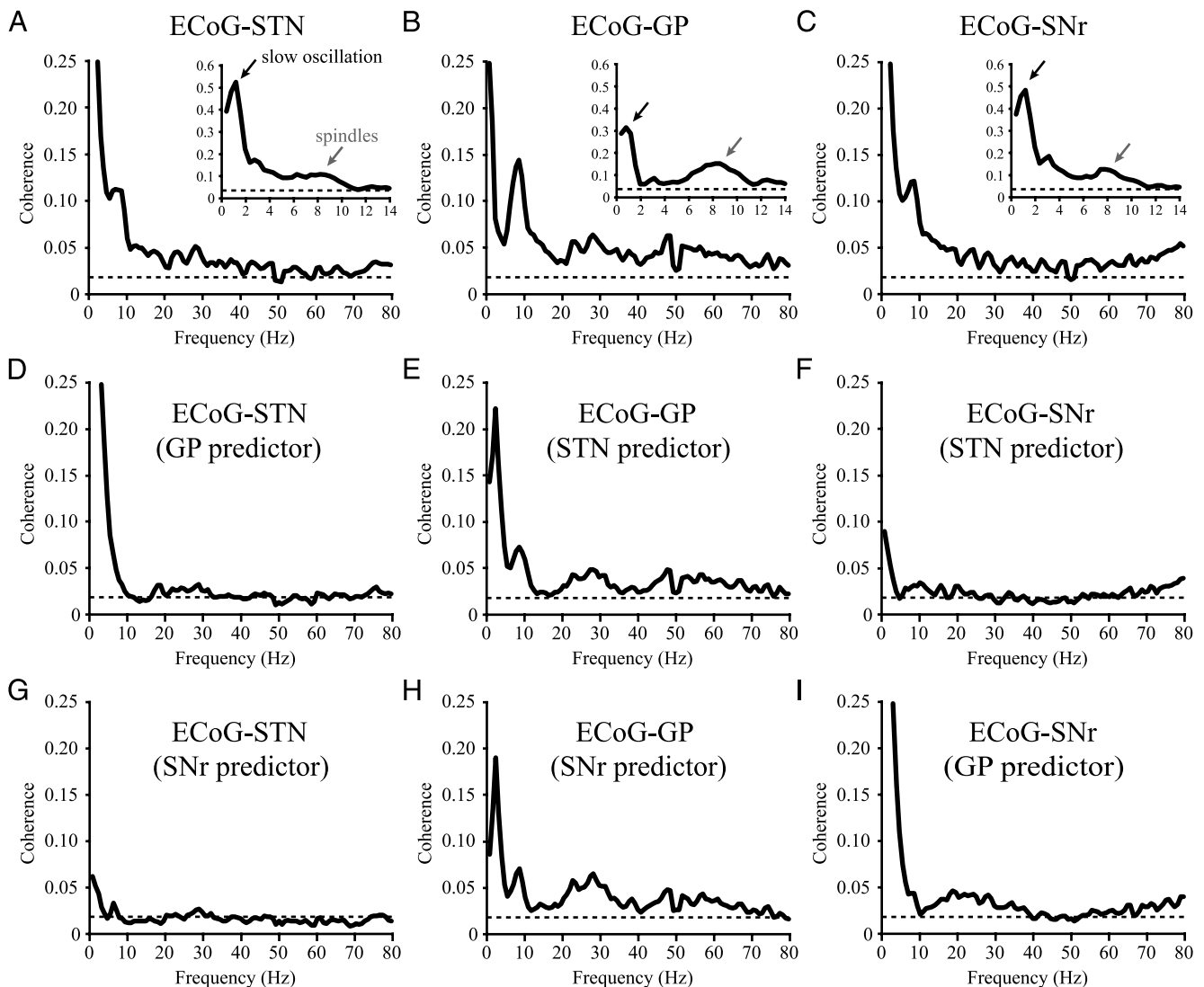


FIG. 5. Coherent oscillatory population activity in cortex and basal ganglia during robust slow-wave activity is largely confined to frequencies associated with the slow oscillation ( $\sim 1$  Hz) and spindle oscillations (7–12 Hz). A–C: coherence spectra between ECoG and LFPs in STN (A), GP (B), and SNr (C). In each case, most of the significant coherence in the 0–80 Hz range was contained in major peaks at about 1 Hz and between 7 and 12 Hz, consistent with the ubiquitous presence of the slow oscillation and spindle activity during SWA. *Insets*: peaks in coherence at about 1 Hz (black arrow) and at spindle frequencies (gray arrow) at higher frequency resolution. The peak in the coherence spectrum of ECoG-GP activity at about 1 Hz (B) was significantly smaller than corresponding peaks in the coherence spectra of ECoG-STN and ECoG-SNr activities (A and C). In contrast, coherence at spindle frequencies was significantly greater between ECoG and GP than between ECoG and STN or SNr. D–I: partial coherence spectra of oscillatory activity in ECoG and LFPs. Partial coherence analysis revealed that when the GP-LFP signal was used as the predictor for coherent activity between ECoG and STN-LFP, the clearly defined peak in coherence at spindle frequencies, but not the peak at about 1 Hz, was lost from the coherence spectrum (D). In contrast, the use of SNr-LFP as the predictor led to an almost complete loss of significant coherence between ECoG and STN-LFP (G). STN-LFP (E) and SNr-LFP (H) signals were not effective predictors of coherence between ECoG and GP-LFP, as shown by the relatively small changes in the coherence plot after partial coherence analysis. In agreement with findings in STN and GP, the coherent activity in ECoG and SNr-LFP was much more sensitive to the use of STN-LFP as a predictor (F) compared with GP-LFP as a predictor (I). Main spectral plots in A to I are grand averages from the 12 animals that were computed using data from two 80 s epochs of slow-wave activity per animal (512 data points per FFT block; 0.78 Hz resolution). *Insets* in A–C are higher-resolution spectra (1024 data points; 0.39 Hz resolution) derived from the same data. Dashed lines indicate 95% confidence levels.

ization with the GP-LFP as predictor (Fig. 6, D and I, respectively). However, the converse was not true; partialization of ECoG-GP coherence with STN or SNr as the predictors led to only modest changes in coherence at these high frequencies (Fig. 6, E and H, respectively). Partialization of ECoG-SNr coherence with STN as predictor, and partialization of ECoG-STN coherence with SNr as predic-

tor, both led to significant reductions in coherence (Fig. 6, F and G, respectively). Thus, in marked contrast to coherence during SWA, the partial spectra in Fig. 6, D–I imply that, during the activated state, prevalent activity in the cortex–STN–SNr axis is shared with GP, although, again, some coherent activity in the loop between cortex and GP was not shared with either STN or SNr.

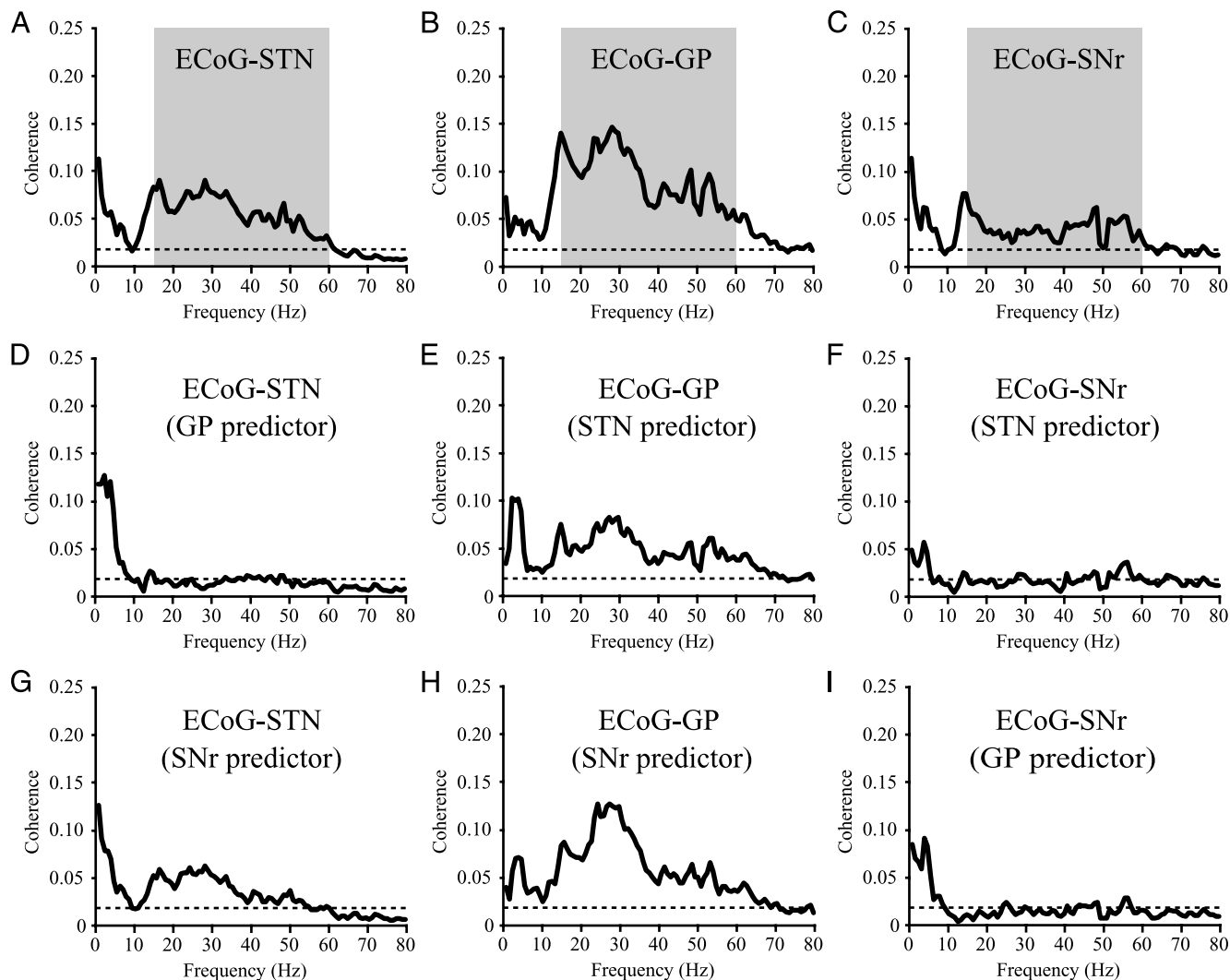


FIG. 6. Coherent oscillatory population activity in cortex and basal ganglia during global activation is largely confined to  $\beta$ - (15–30 Hz) and  $\gamma$  (30–60 Hz) range frequencies. *A–C*: coherence spectra between ECoG and LFPs in STN (*A*), GP (*B*), and SNr (*C*). In each case, much of the significant coherence in the 0–80 Hz range was contained in the  $\beta$ - and  $\gamma$ -frequency bands (light gray boxes in *A–C*), consistent with the obliteration of slow-wave activity and the increased presence of high-frequency oscillations during global activation. Note, however, that coherence between ECoG and SNr-LFP (*C*) at these high frequencies was lower compared with ECoG-STN coherence and ECoG-GP coherence (*A* and *B*). *D–I*: partial coherence spectra of oscillatory activity in ECoG and LFPs. Partial coherence analysis revealed that the use of the GP-LFP as a predictor (*D*), but not the use of SNr-LFP as the predictor (*G*), led to an almost complete loss of significant coherence between ECoG and STN-LFP in the  $\beta$ - and  $\gamma$ -frequency bands. Similarly, the STN-LFP (*E*), but not the SNr-LFP (*H*), was an effective predictor of coherent activity between ECoG and GP-LFP at these high frequencies. Temporal coupling of high-frequency activity in ECoG and SNr-LFP was sensitive to the use of either STN-LFP (*F*) or GP-LFP (*I*) as a predictor of activity. Spectral plots in *A* to *I* are grand averages from the 12 animals that were computed using one 80 s data segment of pinch-evoked activity per animal (512 data points per FFT block; 0.78 Hz resolution). Dashed lines indicate the 95% confidence levels.

#### Quantitative differences in the organization of coherence between ECoG and basal ganglia LFPs according to brain state, frequency, and recording site

Changes in the organization of coherent activity in cortex and basal ganglia with brain state (2 levels: SWA and global activation), frequency band (2 levels: 0.8–1.5 and 15–60 Hz), and partialization (no partialization and partialization with the remaining two basal ganglia nuclei) were objectively and quantitatively assessed by separate GLMs for each basal ganglia nucleus. The results are summarized in Table 1. The GLMs confirmed that all 3 main effects, as well as second- and third-order interactions, were highly significant for ECoG-STN

coherence and ECoG-SNr coherence. In the case of ECoG-GP coherence, there was no significant effect of partialization with STN or SNr signals, either as a main effect or through interaction with other factors (although note that the slow-wave band used tended to exclude some of the coherent activity between cortex and GP during SWA; see above). The other main effects and the interaction between brain state and frequency band were significant.

Post hoc *t*-test verified that partialization of the SWA-related coherence (0.8–1.5 Hz) between ECoG and STN and between ECoG and SNr with, respectively, SNr and STN predictors, significantly reduced coherence in both cases (Fig. 7, *A* and *C*,

TABLE 1. Repeated-measures general linear model (GLM) of changes in coherence between ECoG and basal ganglia LFPs

	STN		GP		SNr	
	F [df]	P value	F [df]	P value	F [df]	P value
Partialization	49.7 [2,20]	<0.001	3.9 [2,20]	(NS)	28.7 [2,20]	<0.001
State	16.0 [1,10]	0.009	25.3 [1,10]	0.003	58.6 [1,10]	<0.001
Frequency	63.9 [1,10]	<0.001	15.7 [1,10]	0.009	97.7 [1,10]	<0.001
Partial × State	41.8 [2,20]	<0.001	1.4 [2,20]	(NS)	11.8 [2,20]	0.009
Partial × Frequency	34.8 [2,20]	<0.001	1.4 [2,20]	(NS)	24.6 [2,20]	<0.001
State × Frequency	33.4 [1,10]	<0.001	43.3 [1,10]	<0.001	47.7 [1,10]	<0.001
Partial × Frequency × State	32.6 [2,20]	<0.001	3.2 [2,20]	(NS)	21.5 [2,20]	0.001

Three main effects were considered: partial coherence (3 levels: no partialization, and partialization with the remaining 2 basal ganglia recording sites), brain state (2 levels: SWA and global activation) and frequency band (2 levels: slow-wave oscillations [0.8–1.5 Hz] and high-frequency oscillations [15–60 Hz]). Separate models were run for coherence between cortex and STN, cortex and GP, and between cortex and SNr. Differences were considered significant when  $P \leq 0.01$ . df, degrees of freedom; NS, not significant.

respectively). In contrast, partialization with GP as predictor had no effect on this low-frequency coherence (Fig. 7, A and C). Furthermore, STN and SNr were not efficient predictors of ECoG-GP coherence (Fig. 7B), confirming that the coherence loop between cortex and STN and the loop between cortex and SNr were functionally related, yet apparently independent of the coherence loop between cortex and GP. During global activation, the high-frequency coherence (15–60 Hz) between ECoG and STN was significantly reduced by partialization with both SNr and GP predictors (Fig. 7D), whereas the high-frequency coherence between ECoG and SNr was significantly reduced by partialization with STN and GP as predictors (Fig. 7F). This adds further weight to the finding that some of the activity in the cortex–STN–SNr axis is shared with GP during activation, when coherence is limited to higher frequencies. Under these circumstances, partialization with a GP predictor reduces ECoG–STN coherence to a greater extent than partialization with a SNr predictor (Fig. 7D). Moreover, much of the coherence within the cortex–GP loop remains independent of temporally coupled activity in STN and SNr during activation, as indicated by the lack of significant effects of predictors of ECoG–GP coherence (Fig. 7E). In short, during activation, coherent activity in the cortex–STN–SNr axis may be shared with GP, but the bulk of coherence between cortex and GP remains restricted to this loop. There were no differences after the use of predictors in the high-frequency bands during robust SWA or the low-frequency band during global activation (results not shown).

#### Changes in the pattern of basal ganglia LFPs with brain state are associated with alterations in local unit activity

The firing properties of single units in GP, STN, and SNr during SWA and global activation are summarized in Table 2, and are similar to those reported by Magill et al. (2001). Unit activity in STN was closely related to ongoing LFP oscillations, with discharge primarily occurring near the negative troughs of the ~1 Hz oscillation in the LFP (Fig. 2). Although STN neurons predominantly fired during the negative phases of the slow oscillation in the LFP, discharges also occurred rarely during positive peaks (Fig. 2). All STN neurons exhibited a significant low-frequency oscillation in their spike trains (*inset* of Fig. 4D). In contrast, GP neurons and SNr neurons exhibited more regular (tonic) firing patterns during SWA (Fig. 2, *insets* of Fig. 4, H and L), as shown by significantly lower CVs, so

that the relationship between single-unit activity and ongoing LFP oscillations was less marked than that in STN.

Changes in the activity profiles of the ECoG and LFPs after sensory-evoked global activation were immediately reflected at the single-cell level by alterations in the rate and pattern of unit activity in basal ganglia (compare Figs. 2 and 3). On average, the firing rate of STN units was significantly increased and the firing pattern became significantly more regular during global activation (Table 2). The firing rates of both GP and SNr units were also significantly increased during global activation; alterations in firing pattern were minor and were evident as small changes in CVs (Table 2). In agreement with previous studies (Magill et al. 2000; Ryan et al. 1992), correlations of STN, GP, and SNr unit activities on the low millisecond time scale (<10 ms) were not observed during either SWA or global activation.

#### Single-unit activity and LFPs in the basal ganglia are correlated during SWA

Changes in LFPs were accompanied by changes in the discharge pattern of single units. This circumstantial association between LFPs and single-unit discharge pattern could be strengthened by the demonstration of a linear relationship between these variables. However, with one important exception, the utility of analyses of the correlation or coherence between units and LFPs recorded through the same electrode is limited by overlaps in the frequency content of the 2 signals, which may lead to the spurious detection of temporal coupling. The exception is the low-frequency activity (~1 Hz) evident in LFPs during SWA. In this case, cumulant density estimates of single-unit and LFP activities demonstrated an unambiguous correlation between unit activity and LFPs in STN (Fig. 4D), and, to a lesser extent, GP and SNr (Fig. 4, H and L). The relatively weak correlations between units and LFPs in GP and SNr might have been a persistent feature throughout the record or may have arisen because of the inclusion of periods of weak low-frequency oscillations in the spike trains of neurons, as sometimes seen after supplementary doses of ketamine, which promotes the emergence of low-frequency oscillatory activity (Magill et al. 2000). Our analysis cannot distinguish these 2 possibilities, but nevertheless, these results serve to show that, during SWA, single-unit activity in GP and SNr can be temporally coupled, albeit weakly or episodically, to ongoing LFP oscillations, whereas single-unit activity in STN remains strongly coupled to LFP oscillations.

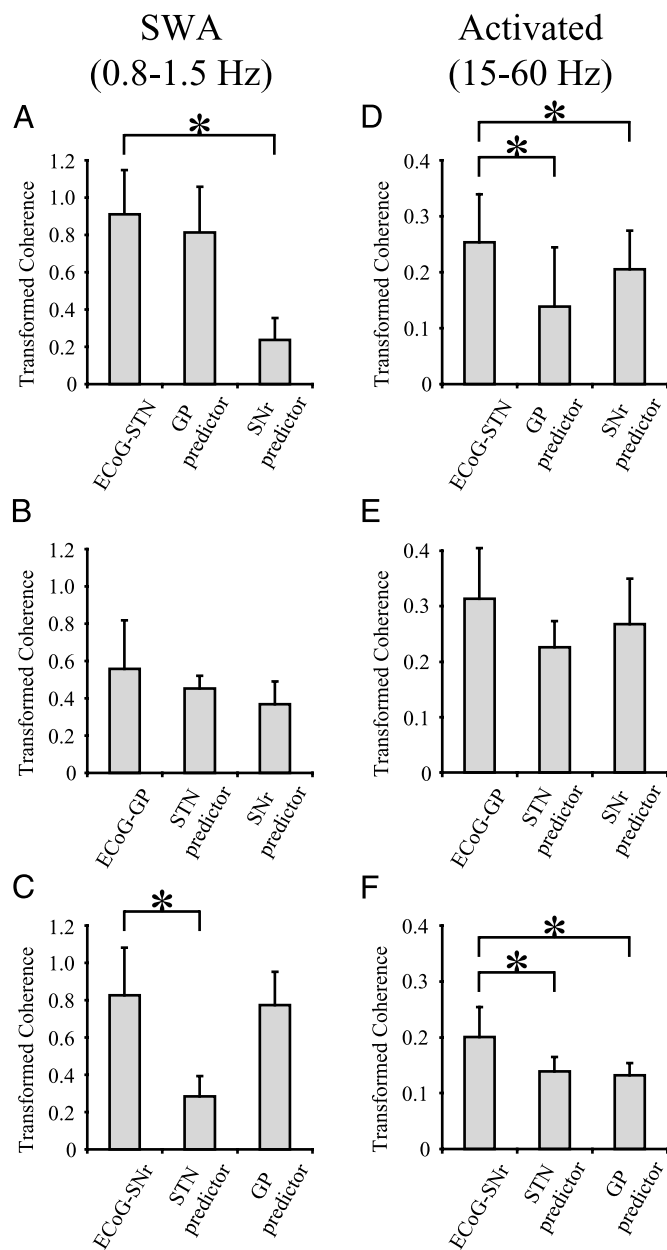


FIG. 7. Summary of changes in coherent activity in the cortex and basal ganglia in the slow-wave frequency band (0.8–1.5 Hz) during robust SWA (A, B, C) and in the combined  $\beta$ - and  $\gamma$ -frequency bands (15–60 Hz) during global activation (D, E, F). Bar charts and error bars represent mean Fisher-transformed coherence values and their SDs, respectively. Asterisks show significant differences in coherence (post hoc 2-tailed *t*-test; significant when  $P \leq 0.01$ ). A: slow-wave activity in ECoG was highly coherent with that in STN-LFP, but only SNr-LFP was an effective predictor of this coherence. B: coherence between ECoG and GP-LFP at these low frequencies was significantly less prominent compared with coherence between ECoG and STN-LFP or SNr-LFP. Neither STN-LFP nor SNr-LFP was a significant predictor of temporal coupling between ECoG and GP-LFP. C: slow-wave activity in ECoG was highly coherent with that in SNr-LFP, and only STN-LFP was a good predictor of coherence. D: during the activated brain state, both GP-LFP and SNr-LFP (although to a lesser extent) were significant predictors of coherence between ECoG and STN-LFP at high frequencies (15–60 Hz). Note different scales in A and D. E: highest coherence in the 15–60 Hz band was between ECoG and GP-LFP. GLM (see Table 1) indicated that partialization of ECoG-GP coherence with either STN-LFP or SNr-LFP as predictor led to no significant changes in coherence. F: coherence between ECoG and SNr-LFP at these high frequencies was significantly less than the coherence between ECoG and STN-LFP or GP-LFP. Local field potentials in STN and GP were both equally effective predictors of coherence between ECoG and SNr-LFP.

## DISCUSSION

The main findings of this study are that coherent oscillations are present in LFPs recorded in cortico-basal ganglia circuits. The frequency of coherent oscillations in cortico-basal ganglia circuits depends on brain state and varies across BG nuclei.

### Interpretation of LFP activity in the basal ganglia

The principal aim of the current work was to gain insight into the nature of functional connectivity between neuronal populations in cortico-basal ganglia circuits. As such, our conclusions depend on whether LFPs can be considered to represent the synchronized activity of local populations of presynaptic and/or postsynaptic neuronal elements. There is good evidence that the LFP activity recorded in the cortex is representative of aggregate or synchronous activity in local neuronal populations (Baker et al. 1997; Creutzfeldt et al. 1966; Donoghue et al. 1998; Frost 1968; Mitzdorf 1985; Murthy and Fetz 1992, 1996; Steriade 2000). The basal ganglia do not share the laminar structure seen in the cortex, but nevertheless there is evidence that LFPs recorded in these nuclei may also reflect synchronized population activity (Courtemanche et al. 2003; Goto and O'Donnell 2001; Levy et al. 2002; Magill et al. 2004). Two aspects of the present results lend further support to this. First, oscillatory LFPs were clearly coherent in distant but connected sites, such as STN and cortex, suggesting that they are at least partly associated with synchronized presynaptic and/or postsynaptic effects. Similar arguments have been made with respect to LFPs recorded in the BG of humans (Brown et al. 2001; Marsden et al. 2001; Williams et al. 2002). Second, in SWA, where action potential-LFP correlations are unambiguous, unit activity was phase-locked to the LFP in STN, and to a lesser extent in GP and SNr (also see Magill et al. 2004).

It is unlikely that LFPs recorded in the BG were contaminated by the volume conduction of cortical potentials, which would lead to inflated measures of the coherence between cortex and BG, for several reasons. During SWA, units were correlated with LFPs, indicating that local currents are timed to elicit phase-locked variations in the firing of neurons. Coherence varied across frequencies, whereas volume-conducted potentials should be equally represented at different frequencies. Power and coherence profiles of LFPs varied across different BG nuclei, and partialization had different and incomplete effects on coherence, both of which argue against a common source of contamination. Consistent with the small temporal offsets of the cumulant density estimates illustrated in Fig. 4, we previously showed that the directed transfer function between cortical and BG activity involves asymmetrical driving (Sharott et al. 2003), rather than the symmetrical effects that would be expected from volume-conducted potentials. Furthermore, using a similar paradigm, we demonstrated that LFPs evoked in cortex and STN by cortical stimulation are not closely related (Magill et al. 2004).

### Neural basis of coherent oscillatory activity in cortex and basal ganglia

The ECoGs of anesthetized rats were dominated by a slow oscillation ( $\sim 1$  Hz) that grouped higher frequency rhythms, including prominent spindle oscillations, and was similar to

TABLE 2. *Firing properties of single units in basal ganglia during slow-wave activity and global activation*

	STN		GP		SNr	
	SWA	Activation	SWA	Activation	SWA	Activation
Total number of neurons <sup>a</sup>	11	11	9	9	11	11
Number of LFO neurons <sup>b</sup>	11	0	0	0	0	0
Firing rate (Hz)	8.4 ± 3.7	14.6 ± 6.1*	21.9 ± 6.3†	30.1 ± 8.0*†	27.0 ± 11.1†	37.2 ± 13.2*†
Coefficient of variation	1.28 ± 0.34	0.53 ± 0.10*	0.25 ± 0.05†	0.21 ± 0.07†	0.24 ± 0.05†	0.23 ± 0.06†

Values are means ± SD. The same neurons were compared in both activity states. Low-frequency oscillatory (LFO) neurons were defined as such when their firing displayed a significant, low-frequency (<1.5 Hz) oscillatory component. \*Significantly different compared to activity of same type of neuron during SWA. †Significantly different compared to activity of STN neurons during same brain state.

that previously described in naturally sleeping or anesthetized rats, cats, and humans (Magill et al. 2000, 2001; Steriade 2000; Urbain et al. 2000). This slow oscillation is generated by synchronous and rhythmic depolarizing and hyperpolarizing events in principal cortical neurons (Steriade 2000; Stern et al. 1997). During SWA, the active components of low-frequency cortical rhythms were closely associated with the burst-like discharges and low-frequency oscillations of single STN neurons. It is thus likely that rhythmic and synchronized cortical input to the STN resulted in periodic depolarization of (and thus increased discharge of) many STN neurons in unison. Indeed, the firing of neighboring STN neurons has been shown to be synchronously phase-locked during SWA (Magill et al. 2000; Ryan et al. 1992). Because LFPs reflect synchronized, subthreshold postsynaptic currents better than action currents (Hubbard et al. 1969; Mitzdorf 1985), the prominent negative deflections in STN-LFPs were probably the result of the synchronized depolarization of neurons by cortical inputs. These periodic depolarizations resulted in the phase-locked discharges of STN neurons. In agreement, distinct LFPs evoked in the STN by cortical stimulation are phase-locked to, but are not dependent on, the discharges of neighboring neurons (Magill et al. 2004).

In contrast to observations in STN, unit activity in GP and SNr was more regular in nature and was less strongly entrained by concurrent cortical SWA. This is despite the fact that both sites receive inputs from STN and striatum, neurons of which often fire in phase with SWA (Goto and O'Donnell 2001; Magill et al. 2000, 2001; Stern et al. 1997). The translation of presynaptic activity into postsynaptic discharge in GP/SNr is therefore complex and partly nonlinear (Hanson and Jaeger 2002). Accordingly, the LFPs in these structures could either reflect presynaptic current flows or, more likely, summated postsynaptic currents that manifest as oscillations in the LFP but which fail to elicit more than minor fluctuations in firing rate (Hubbard et al. 1969; Mitzdorf 1985). In support of this, it has recently been shown that the dendrites of GP neurons receiving subthreshold inputs are functionally uncoupled from the somata of the same neurons (Hanson et al. 2004).

Global activation was associated with a reduction in low-frequency rhythms and increases in the power and coherence of high-frequency oscillations in  $\beta$ - and  $\gamma$ -frequency ranges in the ECoG and LFPs. The effects of global activation were similar to those elicited by the midbrain reticular activating system, which is known to increase cortical activity and promote synchronous, high-frequency oscillations (Munk et al. 1996; Steriade 2000). Thus as with SWA, changes in activity in the BG may be driven, at least in part, by the cortex, although

excitatory subcortical afferents may also contribute to responses (see Magill et al. 2001). These changes were reflected in single-unit activity in BG as increases in the mean firing rates of all neurons and the abolition of low-frequency oscillatory firing of STN neurons. However, it proved impossible to determine unambiguously whether high-frequency LFP activity was correlated with local unit activity recorded through the same electrode because of the overlapping frequency bands of action potential discharge and high-frequency LFP oscillations.

Although unit activity and LFPs both changed on activation, suggesting a relationship, evidence of strict temporal correlations between units was not apparent. A lack of correlations on the low millisecond time scale (<10 ms) suggests that the recorded neurons were not monosynaptically connected (Abelès 1982). Evidence for correlations on a longer time scale is often not forthcoming in the absence of a strong sensory input, a clear behavioral context, or disease. Studies in awake and anesthetized animals have shown that high-frequency oscillations can be effete and focal in nature, especially in sensorimotor systems (Donoghue et al. 1998; MacKay 1997; Murthy and Fetz 1992, 1996). Indeed, correlations between units, or between units and LFPs, are sometimes elusive, perhaps as a consequence of the rapid recruitment of neurons to, and release from, the population oscillation (Donoghue et al. 1998; Murthy and Fetz 1992, 1996). For these reasons, current statistical methods may neglect subtle or dynamic correlations.

#### *Organization of coherent oscillatory activity in cortex and basal ganglia*

The topography and preferred frequency of coherent activity in the cortex and basal ganglia was dynamic, exhibiting a strong dependency on brain state. It was not possible using our analyses to ascribe direction to the coherence described here. The coherence between cortex and BG nuclei is therefore described in terms of distributed and shared "loops." Coherence and partial coherence analyses showed that, during SWA, cortex was temporally coupled to the STN and SNr in highly coherent loops that formed a single functional axis. Cortex was also tightly coupled to the GP, but in an axis distinct from that containing the more strongly coupled STN and SNr. During global activation, cortex was temporally coupled to the STN, GP, and, to a lesser extent, the SNr by loops that formed a single functional axis. In addition, the cortex was closely coupled to the GP alone in another, functionally distinct axis.

The results are compatible with two major conduits of cortical influence over the BG. During SWA, the STN and SNr were temporally coupled at low frequencies to cortex, but not

to the GP, suggesting that, in accordance with past studies of unit activity (Magill et al. 2000, 2001), the STN and SNr may be predominantly driven through the direct cortico-subthalamic projection during SWA. During global activation, high-frequency oscillatory activities in the STN, SNr, and cortex were coherent with one another and with activity in the GP, which raises the possibility that activity of higher frequency may reach the BG predominantly by the cortico-striatal projection to the GP. Indeed, this may also be true of the spindle activity recorded during SWA, which seemed to be shared between the cortex, STN, SNr, and GP, in contrast to the activity at around 1 Hz. At first glance, it seems paradoxical that the GABAergic (presumably inhibitory) projection neurons in the GP could be involved in the propagation of high-frequency activity. However, GABAergic neurons can be as important as excitatory neurons in driving and sculpting population oscillations, both within the BG and in other regions of the brain (Bevan et al. 2002; Klausberger et al. 2003; Whittington and Traub 2003). The division of cortico-basal ganglia information flow into trans-subthalamic and trans-striatal pathways, which thereafter converge at the level of the output nuclei, has already been suggested based on single-unit recordings (Fujimoto and Kita 1992, 1993; Kolomiets et al. 2003; Maurice et al. 1999; Nambu et al. 2000, 2002). It is important to note, however, that the relationships described here may not hold for all cortical areas. Indeed, relationships may depend on the relative influences of trans-striatal and trans-subthalamic pathways, the latter of which is more restricted in terms of contributing cortical regions (Smith et al. 1998). With this caveat in mind, the current data still serve to highlight important new relationships between the BG and a region of frontal cortex that directly projects to both striatum and STN (Fujimoto and Kita 1993; Kolomiets et al. 2003; Magill et al. 2004; Smith et al. 1998).

In summary, the data suggest the existence of two major pathways underlying cortical influence over the BG. Although these pathways have partly overlapping spheres of influence, each favors activities of different frequency. This hypothesis merits further investigation, particularly through simultaneous recordings of LFPs in STN and striatum during SWA and cortical activation. Equally, the role of synchronization in cortico-basal ganglia circuits in behavior has yet to be firmly established. Nevertheless, it is of interest that  $\gamma$ -oscillations have recently been demonstrated in the STN of the alert and mobile rat (Brown et al. 2002), whereas task-related  $\beta$ -oscillations are known to occur throughout the striatum of awake monkeys (Courtemanche et al. 2003). Moreover, the frequency range of coherent activity during global activation is similar to that of (levodopa-responsive) EEG-STN and EEG-GPi coherence in patients with Parkinson's disease (Marsden et al. 2001; Williams et al. 2002).

#### *Implications for information processing in cortico-basal ganglia circuits*

The present data show that the BG oscillate together with the cortex, and that coherent oscillatory activity in cortico-basal ganglia circuits is dynamically and complexly organized. As such, these findings support an extension to classic models of BG function, which posit that simple changes in the rates of firing of neurons underlie behavior (Albin et al. 1989; DeLong 1990; but see Wichmann and DeLong 1996). The existence of

complex, brain state-dependent synchronizations of neuronal ensembles in different frequency bands raises the possibility that synchronization itself may be mechanistically important in the organization of BG function, paralleling its putative roles in cortex (Engel and Singer 2001; Engel et al. 2001; MacKay 1997; Pesaran et al. 2002). Synchronization at subthreshold and suprathreshold levels might provide complex "carrier signals" used by populations of BG neurons to process, encode, and disseminate information. In addition, functional coupling of cortico-basal ganglia circuits through coherent oscillations may facilitate the binding together of distributed neural assemblies during, for example, sensory-motor integration (Cassidy et al. 2002; Engel and Singer 2001; Engel et al. 2001; MacKay 1997; Pesaran et al. 2002; Roelfsema et al. 1997). It follows that dysfunctional coupling of appropriate and/or inappropriate oscillatory population activity may underlie, or at least contribute to, dysfunction in BG diseases. In support of this, aberrant temporal couplings and abnormal oscillatory activities have been frequently observed in cortico-basal ganglia circuits in Parkinson's disease and its models (Bergman et al. 1998; Bevan et al. 2002; Boraud et al. 2002; Brown 2003; Levy et al. 2000, 2002; Liu et al. 2002; Marsden et al. 2001; Wichmann and DeLong 1996; Williams et al. 2002).

#### ACKNOWLEDGMENTS

We are grateful to Drs. M. Bevan, J. Csicsvari, T. Klausberger, and M. Capogna for valuable comments on an early version of this manuscript. We thank L. Norman, C. Francis, and B. Micklem for technical assistance.

#### GRANTS

This work was supported by the Medical Research Council UK and the Brain Research Trust. P. J. Magill holds a *Fellowship by Examination* at Magdalen College, Oxford.

#### REFERENCES

- Abeles M.** Quantification, smoothing, and confidence limits for single-units' histograms. *J Neurosci Methods* 5: 317–325, 1982.
- Albin RL, Young AB, and Penney JB.** The functional anatomy of basal ganglia disorders. *Trends Neurosci* 12: 366–375, 1989.
- Alexander GE and Crutcher MD.** Functional architecture of basal ganglia circuits: neural substrates of parallel processing. *Trends Neurosci* 13: 266–271, 1990.
- Baker SN, Olivier E, and Lemon RN.** Coherent oscillations in monkey motor cortex and hand muscle EMG show task-dependent modulation. *J Physiol* 501: 225–241, 1997.
- Bergman H, Feingold A, Nini A, Raz A, Slovlin H, Abeles M, and Vaadia E.** Physiological aspects of information processing in the basal ganglia of normal and parkinsonian primates. *Trends Neurosci* 21: 32–38, 1998.
- Bevan MD, Magill PJ, Terman D, Bolam JP, and Wilson CJ.** Move to the rhythm: oscillations in the subthalamic nucleus-external globus pallidus network. *Trends Neurosci* 25: 525–531, 2002.
- Bolam JP.** (editor) *Experimental Neuroanatomy*. Oxford, UK: Oxford Univ. Press, 1992.
- Boraud T, Bezaud E, Bioulac B, and Gross CE.** From single extracellular unit recording in experimental and human Parkinsonism to the development of a functional concept of the role played by the basal ganglia in motor control. *Prog Neurobiol* 66: 265–283, 2002.
- Brillinger DR.** *Time Series—Data Analysis and Theory* (2nd ed.). San Francisco, CA: Holden Day, 1981.
- Brown P.** Oscillatory nature of human basal ganglia activity: relationship to the pathophysiology of Parkinson's disease. *Mov Disord* 18: 357–363, 2003.
- Brown P, Kupsch A, Magill PJ, Sharott A, Harnack D, and Meissner W.** Oscillatory local field potentials recorded from the subthalamic nucleus of the alert rat. *Exp Neurol* 177: 581–585, 2002.
- Brown P, Oliviero A, Mazzone P, Insola A, Tonali P, and Di Lazzaro V.** Dopamine dependency of oscillations between subthalamic nucleus and pallidum in Parkinson's disease. *J Neurosci* 21: 1033–1038, 2001.

- Bullock TH.** Signals and signs in the nervous system: the dynamic anatomy of electrical activity is probably information-rich. *Proc Natl Acad Sci USA* 94: 1–6, 1997.
- Buzsáki G.** Theta oscillations in the hippocampus. *Neuron* 33: 325–340, 2002.
- Cassidy M, Mazzone P, Oliviero A, Insola A, Tonali P, Di Lazzaro V, and Brown P.** Movement-related changes in synchronization in the human basal ganglia. *Brain* 125: 1235–1246, 2002.
- Challis RE and Kitney RL.** Biomedical signal processing (in four parts). Part 1: time-domain methods. *Med Biol Eng Comput* 28: 509–524, 1990.
- Contreras D, Destexhe A, Sejnowski TJ, and Steriade M.** Spatiotemporal patterns of spindle oscillations in cortex and thalamus. *J Neurosci* 17: 1179–1196, 1997.
- Courtemanche R, Fujii N, and Graybiel AM.** Synchronous, focally modulated beta-band oscillations characterize local field potential activity in the striatum of awake behaving monkeys. *J Neurosci* 23: 11741–11752, 2003.
- Creutzfeldt OD, Watanabe S, and Lux HD.** Relations between EEG phenomena and potentials of single cortical cells. II. Spontaneous and convulsoid activity. *Electroencephalogr Clin Neurophysiol* 20: 19–37, 1966.
- DeLong MR.** Primate models of movement disorders of basal ganglia origin. *Trends Neurosci* 13: 281–285, 1990.
- Donoghue JP, Sanes JN, Hastopoulos NG, and Gaál G.** Neural discharge and local field potential oscillations in primate motor cortex during voluntary movements. *J Neurophysiol* 79: 159–173, 1998.
- Donoghue JP and Wise SP.** The motor cortex of the rat: cytoarchitecture and microstimulation mapping. *J Comp Neurol* 212: 76–88, 1982.
- Engel AK, Fries P, and Singer W.** Dynamic predictions: oscillations and synchrony in top-down processing. *Nat Rev Neurosci* 2: 704–716, 2001.
- Engel AK and Singer W.** Temporal binding and the neural correlates of sensory awareness. *Trends Cogn Sci* 5: 16–25, 2001.
- Florian G, Andrew C, and Pfurtscheller G.** Do changes in coherence always reflect changes in functional coupling? *Electroencephalogr Clin Neurophysiol* 106: 87–91, 1998.
- Frost JD Jr.** EEG-intracellular potential relationships in isolated cerebral cortex. *Electroencephalogr Clin Neurophysiol* 24: 434–443, 1968.
- Fujimoto K and Kita H.** Responses of substantia nigra *pars reticulata* units to cortical stimulation. *Neurosci Lett* 142: 105–109, 1992.
- Fujimoto K and Kita H.** Response characteristics of subthalamic neurons to the stimulation of the sensorimotor cortex in the rat. *Brain Res* 609: 185–192, 1993.
- Gerfen CR and Wilson CJ.** The basal ganglia. In: *Handbook of Chemical Neuroanatomy 12: Integrated Systems of the CNS III*, edited by Swanson LW, Björklund A, and Hökfelt T. London: Elsevier, 1996, p. 371–468.
- Goto Y and O'Donnell P.** Network synchrony in the nucleus accumbens *in vivo*. *J Neurosci* 21: 4498–4504, 2001.
- Graybiel AM.** Building action repertoires: memory and learning functions of the basal ganglia. *Curr Opin Neurobiol* 5: 733–741, 1995.
- Halliday DM, Conway BA, Farmer SF, and Rosenberg JR.** Load-independent contributions from motor-unit synchronisation to human physiological tremor. *J Neurophysiol* 82: 664–675, 1999.
- Halliday DM, Rosenberg JR, Amjad AM, Breeze P, Conway BA, and Farmer SF.** A framework for the analysis of mixed time series/point process data—theory and application to the study of physiological tremor, single motor unit discharges and electromyograms. *Prog Biophys Mol Biol* 64: 237–278, 1995.
- Hanson JE and Jaeger D.** Short-term plasticity shapes the response to simulated normal and parkinsonian input patterns in globus pallidus. *J Neurosci* 22: 5164–5172, 2002.
- Hanson JE, Smith Y, and Jaeger D.** Sodium channels and dendritic spike initiation at excitatory synapses in globus pallidus neurons. *J Neurosci* 24: 329–340, 2004.
- Hu D, Itoga CA, Tierny PL, Soucy AL, Ghiglieri V, Bergstrom DA, and Walters JR.** Slow oscillations in globus pallidus (GP) local field potential (LFP) in anesthetized rats and mice exhibit coherence with striatal and hippocampal (HP) LFP. *Soc Neurosci Abstr* 28: 765.2, 2002.
- Hubbard JI, Llinás R, and Quastel DMJ.** Extracellular field potentials in the central nervous system. In: *Electrophysiological Analysis of Synaptic Transmission*. London: Edward Arnold, 1969, p. 265–293.
- Johnson DH.** Point process models of single-neuron discharges. *J Comput Neurosci* 3: 275–299, 1996.
- Klausberger T, Magill PJ, Márton LF, Roberts JD, Cobden PM, Buzsáki G, and Somogyi P.** Brain-state- and cell-type-specific firing of hippocampal interneurons *in vivo*. *Nature* 421: 844–848, 2003.
- Kocsis B, Bragin A, and Buzsáki G.** Interdependence of multiple theta generators in the hippocampus: a partial coherence analysis. *J Neurosci* 19: 6200–6212, 1999.
- Kolomiets BP, Deniau JM, Glowinski J, and Thierry AM.** Basal ganglia and processing of cortical information: functional interactions between trans-striatal and trans-subthalamic circuits in the substantia nigra *pars reticulata*. *Neuroscience* 117: 931–938, 2003.
- Korzeniewska A, Manczak M, Kaminski M, Blinowska KJ, and Kasicki S.** Determination of information flow direction among brain structures by a modified directed transfer function (dDTF) method. *J Neurosci Methods* 125: 195–207, 2003.
- Kühn AA, Williams D, Kupsch A, Limousin P, Hariz M, Schneider GH, Yarrow K, and Brown P.** Event-related beta desynchronization in human subthalamic nucleus correlates with motor performance. *Brain* 127: 735–746, 2004.
- Levy R, Ashby P, Hutchison WD, Lang AE, Lozano AM, and Dostrovsky JO.** Dependence of subthalamic nucleus oscillations on movement and dopamine in Parkinson's disease. *Brain* 125: 1196–1209, 2002.
- Levy R, Hutchison WD, Lozano AM, and Dostrovsky JO.** High-frequency synchronization of neuronal activity in the subthalamic nucleus of parkinsonian patients with limb tremor. *J Neurosci* 20: 7766–7775, 2000.
- Liu X, Ford-Dunn HL, Hayward GN, Nandi D, Miall RC, Aziz TZ, and Stein J.** The oscillatory activity in the Parkinsonian subthalamic nucleus investigated using the macro-electrodes for deep brain stimulation. *Clin Neurophysiol* 113: 1667–1672, 2002.
- Lopes da Silva FH, Vos JE, Mooibroek JN, and Van Rotterdam A.** A partial coherence analysis of thalamic and cortical alpha rhythms in dog—a contribution towards a general model of cortical organisation of rhythmic activity. In: *Event Related Changes in Cortical Rhythmic Activities—Behavioural Correlates*, edited by Pfurtscheller G. Amsterdam: Elsevier/North-Holland Biomedical Press, 1980, p. 33–59.
- MacKay WA.** Synchronised neuronal oscillations and their role in motor processes. *Trends Cogn Sci* 1: 176–183, 1997.
- Magill PJ, Bolam JP, and Bevan MD.** Relationship of activity in the subthalamic nucleus-globus pallidus network to cortical electroencephalogram. *J Neurosci* 20: 820–833, 2000.
- Magill PJ, Bolam JP, and Bevan MD.** Dopamine regulates the impact of the cerebral cortex on the subthalamic nucleus-globus pallidus network. *Neuroscience* 106: 313–330, 2001.
- Magill PJ, Sharott A, Bevan MD, Brown P, and Bolam JP.** Synchronous unit activity and local field potentials evoked in the subthalamic nucleus by cortical stimulation. *J Neurophysiol* March 24, 2004; 10.1152/jn.00134.2004.
- Marsden JF, Limousin-Dowsey P, Ashby P, Pollak P, and Brown P.** Subthalamic nucleus, sensorimotor cortex and muscle interrelationships in Parkinson's disease. *Brain* 124: 378–388, 2001.
- Maurice N, Deniau JM, Glowinski J, and Thierry AM.** Relationships between the prefrontal cortex and the basal ganglia in the rat: physiology of the cortico-nigral circuits. *J Neurosci* 19: 4674–4681, 1999.
- Mitzdorf U.** Current-source density method and application in cat cerebral cortex: investigation of evoked potentials and EEG phenomena. *Physiol Rev* 65: 37–100, 1985.
- Munk MH, Roelfsema PR, König P, Engel AK, and Singer W.** Role of reticular activation in the modulation of intracortical synchronization. *Science* 272: 271–274, 1996.
- Murthy VN and Fetz EE.** Coherent 25- and 35-Hz oscillations in the sensorimotor cortex of awake behaving monkeys. *Proc Natl Acad Sci USA* 89: 5670–5674, 1992.
- Murthy VN and Fetz EE.** Synchronization of neurons during local field potential oscillations in sensorimotor cortex of awake monkeys. *J Neurophysiol* 76: 3968–3982, 1996.
- Nambu A, Tokuno H, Hamada I, Kita H, Imanishi M, Akazawa T, Ikeuchi Y, and Hasegawa N.** Excitatory cortical inputs to pallidal neurons via the subthalamic nucleus in the monkey. *J Neurophysiol* 84: 289–300, 2000.
- Nambu A, Tokuno H, and Takada M.** Functional significance of the cortico-subthalamo-pallidal “hyperdirect” pathway. *Neurosci Res* 43: 111–117, 2002.
- Paxinos G and Watson C.** *The Rat Brain in Stereotaxic Coordinates* (2nd ed.). Sydney, Australia: Academic Press, 1986.
- Perkel DH, Gerstein GL, and Moore GP.** Neuronal spike trains and stochastic point processes. II. Simultaneous spike trains. *Biophys J* 7: 419–440, 1967.

- Pesaran B, Pezaris JS, Sahani M, Mitra PP, and Andersen RA.** Temporal structure in neuronal activity during working memory in macaque parietal cortex. *Nat Neurosci* 5: 805–811, 2002.
- Roelfsema PR, Engel AK, König P, and Singer W.** Visuomotor integration is associated with zero time-lag synchronization among cortical areas. *Nature* 385: 157–161, 1997.
- Rosenberg JR, Amjad AM, Breeze P, Brillinger DR, and Halliday DM.** The Fourier approach to the identification of functional coupling between neuronal spike trains. *Prog Biophys Mol Biol* 53: 1–31, 1989.
- Rosenberg JR, Halliday DM, Breeze P, and Conway BA.** Identification of patterns of neuronal activity; partial spectra, partial coherence, and neuronal interactions. *J Neurosci Methods* 83: 57–72, 1998.
- Ryan LJ, Sanders DJ, and Clark KB.** Auto- and cross-correlation analysis of subthalamic nucleus neuronal activity in neostriatal- and globus pallidus-lesioned rats. *Brain Res* 583: 253–261, 1992.
- Sharott A, Magill PJ, Bolam JP, and Brown P.** Direct transfer function analysis of coherent oscillatory field potentials in the cerebral cortex and basal ganglia of the anaesthetised rat. *Soc Neurosci Abstr* 30: 390.13, 2003.
- Smith Y, Bevan MD, Shink E, and Bolam JP.** Microcircuitry of the direct and indirect pathways of the basal ganglia. *Neuroscience* 86: 353–387, 1998.
- Spauschus A, Marsden J, Halliday DM, Rosenberg JR, and Brown P.** The origin of ocular microtremor in man. *Exp Brain Res* 126: 556–562, 1999.
- Steriade M.** Corticothalamic resonance, states of vigilance and mentation. *Neuroscience* 101: 243–276, 2000.
- Stern EA, Kincaid AE, and Wilson CJ.** Spontaneous subthreshold membrane potential fluctuations and action potential variability of rat corticostriatal and striatal neurons in vivo. *J Neurophysiol* 77: 1697–1715, 1997.
- Urbain N, Gervasoni D, Soulière F, Lobo L, Rentéro N, Windels F, Astier B, Savasta M, Fort P, Renaud B, Luppi PH, and Chouvet G.** Unrelated course of subthalamic nucleus and globus pallidus neuronal activities across vigilance states in the rat. *Eur J Neurosci* 12: 3361–3374, 2000.
- Whittington MA and Traub RD.** Interneuron diversity series: inhibitory interneurons and network oscillations *in vitro*. *Trends Neurosci* 26: 676–682, 2003.
- Wichmann T and DeLong MR.** Functional and pathophysiological models of the basal ganglia. *Curr Opin Neurobiol* 6: 751–758, 1996.
- Williams D, Tijssen M, Van Bruggen G, Bosch A, Insola A, Di Lazzaro V, Mazzone P, Oliviero A, Quartarone A, Speelman H, and Brown P.** Dopamine-dependent changes in the functional connectivity between basal ganglia and cerebral cortex in humans. *Brain* 125: 1558–1569, 2002.